Electronic Supplementary Material (ESI) for Journal of Materials Chemistry A

Supporting Information

Nanowire architectures for iodide free dye sensitized solar cells

Venkat Kalyan Vendra,[a] Tu Nguyen,[a] Thad Druffel,[b] Delaina A. Amos,[a] Jacek Jasinski, Mahendra K. Sunkara[a,b,*]

[a] Department of Chemical Engineering, University of Louisville, Louisville, KY 40292, USA.
[b] Conn Center for Renewable Energy Research, University of Louisville, Louisville, KY 40292, USA.
* Corresponding authors email: mahendra@louisville.edu

Table S1 lists the redox potentials and the maximum open circuit potentials that can be obtained from these redox couples.

Table S1. Redox potentials of different redox electrolytes and maximum theoretical open-circuit voltages for titania and tin oxide

Redox electrolyte	Redox potential vs. NHE	Maximum open-circuit voltage for TiO_2	Maximum open-circuit voltage for SnO_2
Ioidide/Tri-iodide	0.50 V	1.0 V	0.60 V
Ferrocene /Ferrocenium	0.62 V	1.12 V	0.72 V
TEMPO/$TEMPO^+$	0.74 V	1.24 V	0.84 V

The higher maximum redox potentials that can be achieved with these redox couples make them promising electrolytes for use in dye-sensitized solar cells (DSCs). It is important to note that proper energetic alignment between the dye and the redox couple is necessary to achieve high performance with these redox electrolytes. Specifically, the HOMO level of the dye should be positive enough such that there is sufficient driving force for the dye regeneration.

Figure S1 compares the current-voltage characteristics of DSCs fabricated with unpassivated SnO_2 NWs and TiO_2 NPs using TEMPO redox electrolyte. The SnO_2 NWs show

enhanced current density and voltage when compared with TiO_2 NPs due to reduced recombination losses and improved charge transport in SnO_2 NWs.

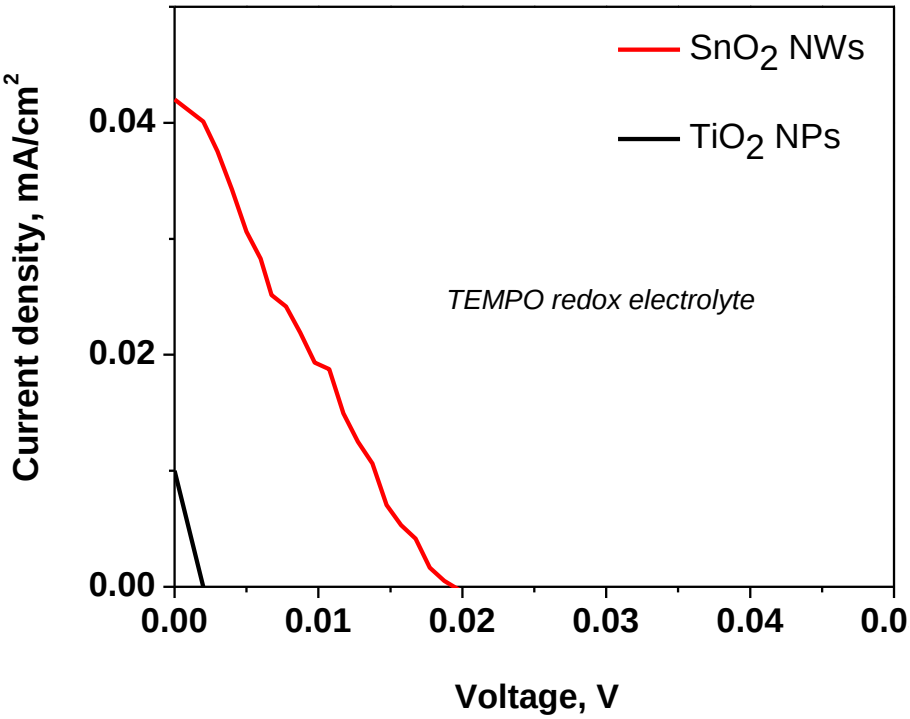

Figure S1. Current-Voltage characteristics of unpassivated tin oxide nanowires and titania nanoparticles with TEMPO redox couple

The lower values of short-circuit density, open-circuit voltage and fill factor when compared with ferrocene redox couple (shown in Figure 2a) could be attributed to the faster recombination kinetics with TEMPO redox couple.

Figure S2b shows the current-voltage characteristics of Al_2O_3 passivated TiO_2 NPs and SnO_2 NWs coated with a 100 nm shell of TiO_2 by atomic layer deposition (Figure S2a). The TEMPO redox couple was used for the experiments.

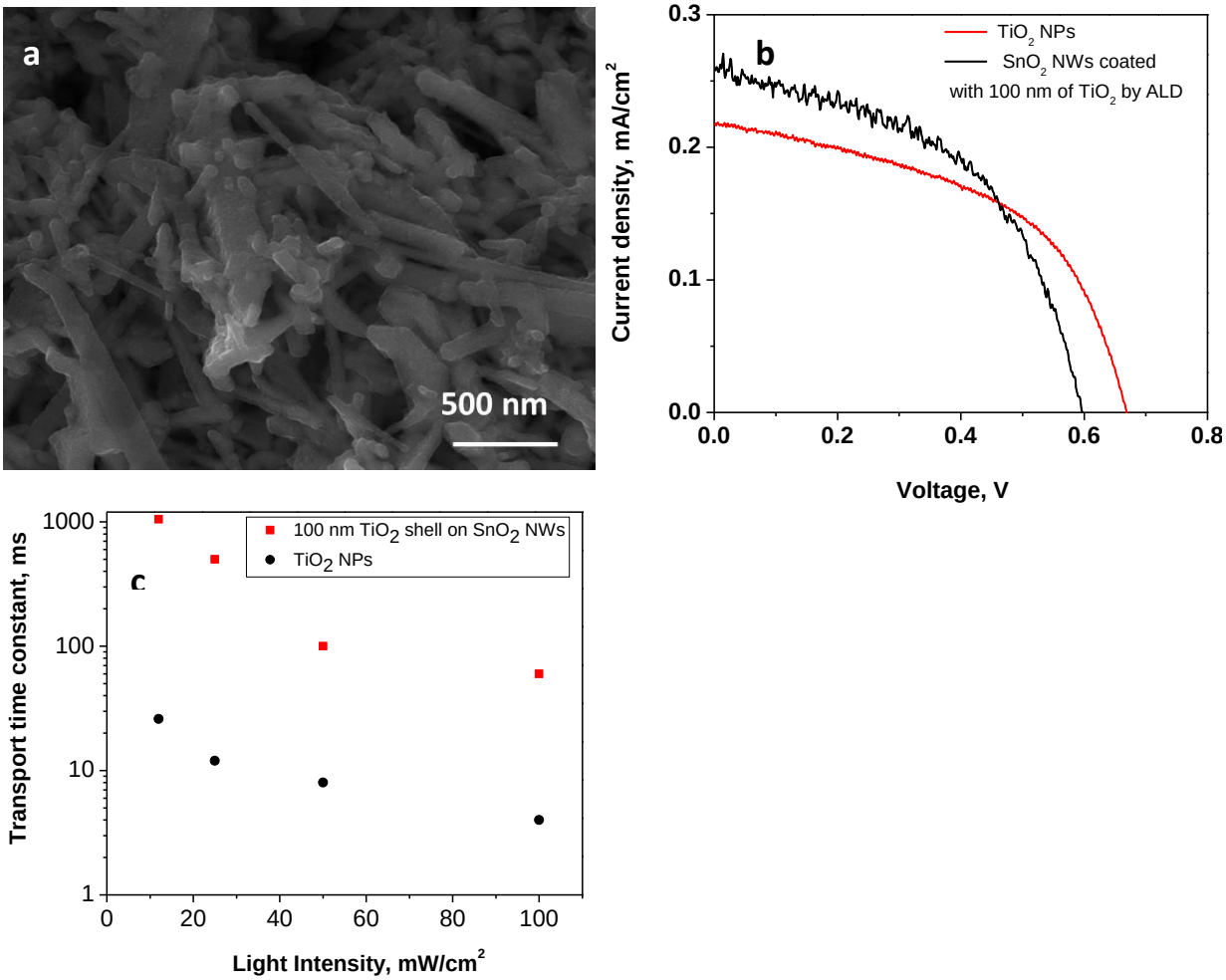

Figure S2 (a) SEM image showing SnO_2 nanowires coating with 100 nm of TiO_2 by atomic layer deposition **(b)** Current-Voltage characteristics of TiO_2 NPs and SnO_2 -TiO_2 core shell NW architectures**(c)** Comparison of transport time constants of TiO_2 NPs and SnO_2 -TiO_2 core shell NW architectures

The enhancement in current density is not as significant as the case of SnO_2 NWs coated with anatase TiO_2 NPs by electrophoretic deposition, where a ten-fold enhancement in current density. This can explained by considering the poor electron transport and high resistivity of amorphous TiO_2.[1] The electrophoretic deposition approach described in this work is much simpler and more effective way to create crystalline shells of titania with good charge transport properties. Further, the increased surface roughness in the case of electrophoretic deposition leads to increased surface area for dye adsorption.

Figure S3 shows the electron transport times and electron lifetimes in rutile TiO_2 NWs, $TiCl_4$ treated rutile NWs and TiO_2 NPs. The characterization was performed using an iodide redox electrolyte without any surface passivation of TiO_2. There is no difference in the electron transport between TiO_2 nanoparticles and single crystal rutile TiO_2 NWs. The presence of a large number of Ti^{+3} trap states in TiO_2 lower the electron mobility and result in slow electron transport in TiO_2 NWs.[2] The electron lifetimes in the rutile TiO_2 NWs were an order of magnitude higher than TiO_2 NPs because of the surface trap state concentration on TiO_2 NWs when compared with TiO_2 NPs.

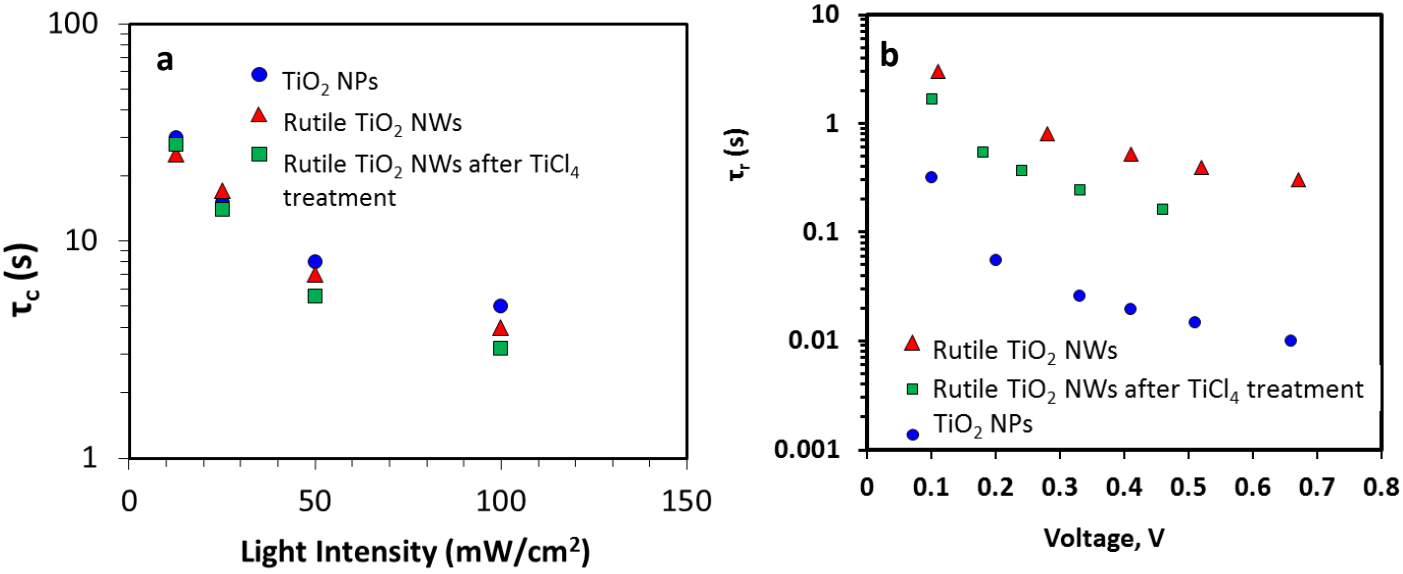

Figure S3. (a) Electron transport and **(b)** electron lifetimes in rutile TiO_2 NWs, $TiCl_4$ treated rutile NWs and TiO_2 NPs characterized using an iodide/triiodide redox couple.

Figure S4 compares the dye adsorption spectrum (in Kubelka-Munk units) for titania NPs and tin oxide NW hybrid architectures after dye adsorption. The hybrid architectures show a significantly low dye adsorption due to the low surface area.

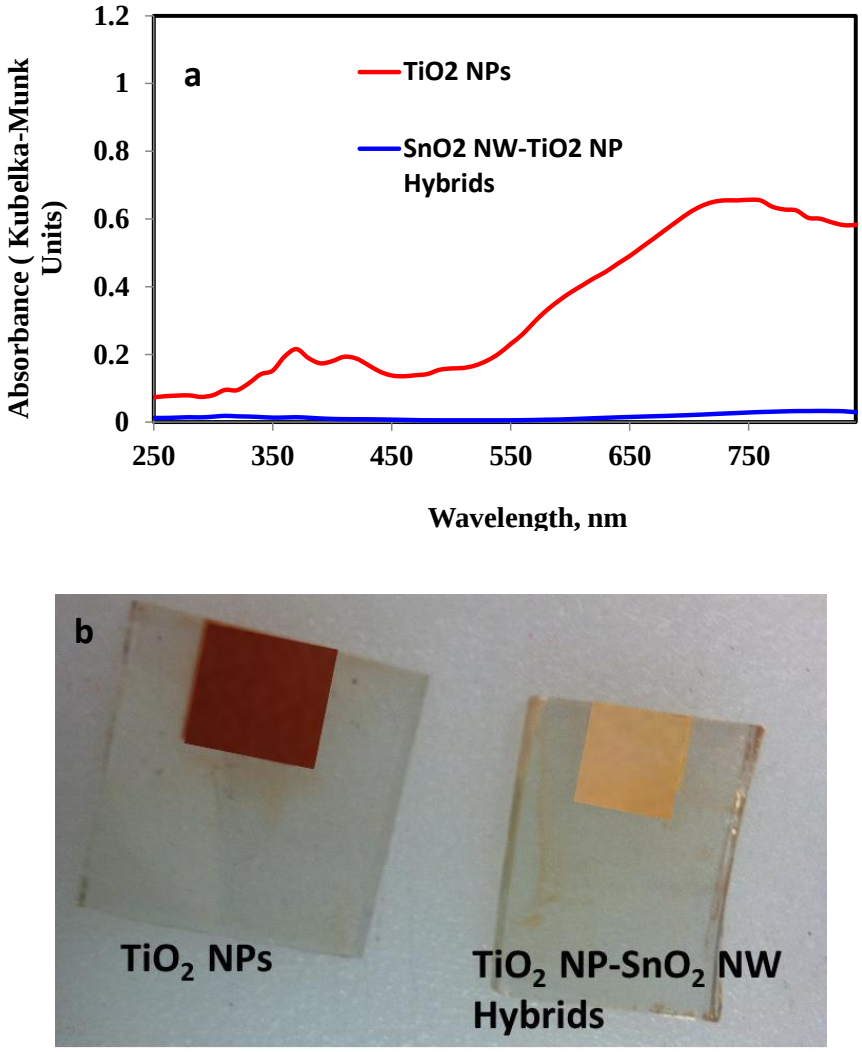

Figure S4. (a) Comparison of absorbance spectrum of the N-719 sensitized TiO_2 NPs and TiO_2 NP-SnO_2 NW Hybrids (b) picture showing TiO_2 NPs and TiO_2 NP-SnO_2 NW Hybrids after sensitization with N-719 dye.

To quantify the dye loading on the TiO2 NPs- SnO2 NW hybrid architectures and titania nanoparticles, dye desorption experiments were performed. The UV-Vis spectrum of N-719 dye solution of different concentrations were measured to obtain a calibration curve (Figure S5).

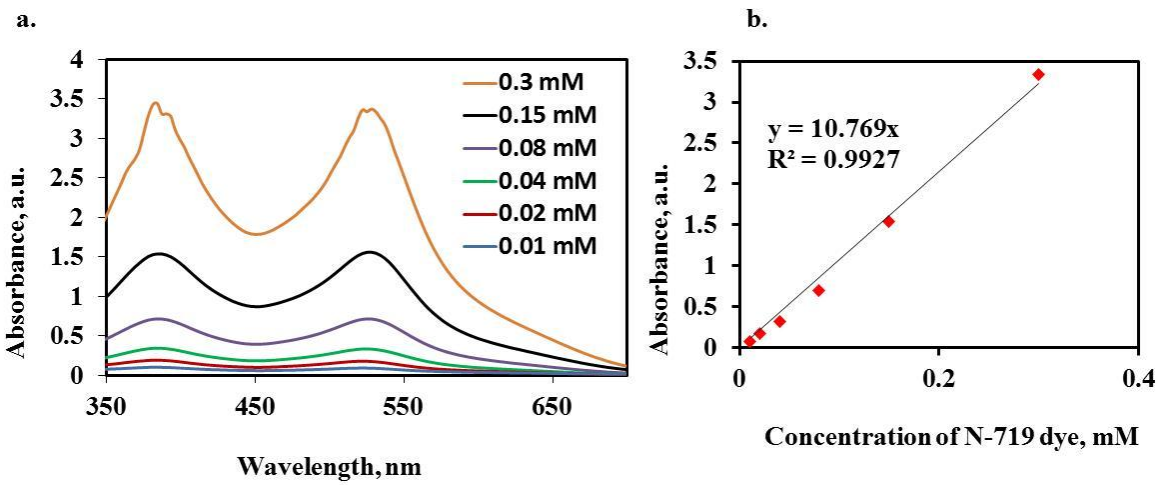

Figure S5 (a) UV-Vis spectra of different concentration of N-719 dye in ethanol and (b) calibration curve obtained from part (a).The absorbance at 531 nm was used to obtain the calibration curve.

The dye desorption experiments were performed by soaking the N-719 sensitized electrodes in 6 mL of 0.1 M NaOH solution for 1h. Table S2 shows the dye loading characteristics and surface area of the different samples. For calculating the surface area, the area of single N-719 dye molecule is taken as 1.6×10^{-18} m^2.[15] In addition the BET surface area of the electrodes was also determined (Micromeritics Tristar 3000).

Table S2. Dye loading characteristics and surface area measurements of different electrodes

Sample	**Dye loading, moles.cm^{-2} of substrate**	**Surface area, m^2/g, (from dye desorption experiments)**	**BET surface area, m^2/g**
TiO_2 NPs	3.8×10^{-7}	82.9	89.4
TiO_2 NP-SnO_2 NW hybrids	1.5×10^{-7}	40.2	33.3
SnO_2 NWs	0.8×10^{-7}	12.1	10.1

Table S3. Photovoltaic characteristics for different electrolytes used with organic dyes

Electrolyte	***Dye***	V_{oc}, **V**	J_{sc}, **mA/cm^2**	% η	***Dye HOMO,* V vs. SHE**	***Electrolyte redox potential,* V vs. SHE**	***Ref.***
Br^-/Br_3^-	*EOSIN-Y*	*0.81*	*4.63*	*2.6*	*1.2*	*1.1*	[3]
$[Fe(CN)_6]^{4-}/^{3-}$	*MK-2*	*0.73*	*5.46*	*2.99*	*0.9*	*0.42*	[4]
$[Co(dtb)_3]^{2+/3+}$	*D35*	*0.7*	*8.5*	*3.0*	*1.1*	*0.6*	[5]
$[Co(phen)_3]^{2+/3+}$	*D35*	*0.92*	*8.2*	*4.5*	*1.1*	*0.6*	[5]
$[Co(dmb)_3]^{2+/3+}$	*D35*	*0.75*	*10.5*	*4.7*	*1.1*	*0.4*	[5]
$TEMPO/TEMPO^+$	*D-149*	*0.83*	*9.4*	*5.4*	*1.1*	*0.8*	[6]
$[Co(bpy)_3]^{2+/3+}$	*D35*	*0.92*	*10.5*	*5.8*	*1.1*	*0.6*	[5]
Fc/Fc^+	Carbz-PAHTDTT	*0.84*	*12.2*	*7.5*	*0.9*	*0.63*	[7]
$[Co(bpy\text{-}pz)_2]^{3+/2+}$	*Y-123*	*0.99*	*13.06*	*10.1*	*1.1*	*0.9*	[8]
I^-/I_3^-	CYC-B11	*0.74*	*20.1*	*11.5*	*1.0*	*0.5*	[9]
$Co^{2+/3+}$ tris(bpy)	YD2-*o*-C8	*0.96*	*17.3*	*12.3*	*0.8*	*0.5*	[10]

Table S4. Photovoltaic characteristics for different electrolytes used with ruthenium dyes

Electrolyte	***Dye***	V_{oc} **V**	J_{sc} **mA/cm^2**	% η	***Dye HOMO,*** **V vs. SHE**	***Electrolyte redox potential,*** **V vs. SHE**	***Ref.***
$[Cu(phen)2]^{2+/+}$	*N-719*	*0.57*	*0.48*	*0.12*	1.12	*0.1*	11
Fc/Fc^{+}	*N-719*	*0.55*	*1.0*	0.33	1.12	*0.63*	7
$[Fe(CN)_6]^{4-/3-}$	*Z-907*	*0.65*	*1.79*	*0.79*	*0.98*	*0.42*	4
Br^{-}/Br_3^{-}	*N-719*	*0.55*	*3.51*	*1.05*	1.12	*1.1*	3
$[Cu(SP)(mmt)]^{0/-}$	*N-719*	*0.66*	*4.4*	*1.3*	1.12	*0.49*	11
$[Cu(dmp)2]^{2+/+}$	*N-719*	*0.79*	*3.2*	*1.4*	1.12	*0.86*	11
[Ni-bis(dicarbodillide)]$^{0/-1}$	*N-719*	*0.64*	*3.76*	*1.5*	1.12	*0.49*	12
Difsulfide/thiolate	*Z-907*	*0.68*	*16.18*	*6.44*	*0.98*	*0.485*	13
I^{-}/I_3^{-}	*N-719*	*0.78*	*16.25*	*9.1*	*1.12*	*0.5*	14

References

1. Law, M.; Greene, L. E.; Johnson, J. C.; Saykally, R.; Yang, P. D., Nanowire dye-sensitized solar cells. *Nature Materials* **2005,** *4* (6), 455-459.
2. Richter, C.; Schmuttenmaer, C. A., Exciton-like trap states limit electron mobility in TiO2 nanotubes. *Nature Nanotechnology* **2010,** *5* (11), 769-772.
3. Wang, Z.-S.; Sayama, K.; Sugihara, H., Efficient eosin Y dye-sensitized solar cell containing Br-/Br3-electrolyte. *The Journal of Physical Chemistry B* **2005,** *109* (47), 22449-22455.
4. Daeneke, T.; Uemura, Y.; Duffy, N. W.; Mozer, A. J.; Koumura, N.; Bach, U.; Spiccia, L., Aqueous Dye-Sensitized Solar Cell Electrolytes Based on the Ferricyanide-Ferrocyanide Redox Couple. *Advanced Materials* **2012,** *24* (9), 1222-1225.

5. Feldt, S. M.; Gibson, E. A.; Gabrielsson, E.; Sun, L.; Boschloo, G.; Hagfeldt, A., Design of organic dyes and cobalt polypyridine redox mediators for high-efficiency dye-sensitized solar cells. *Journal of the American Chemical Society* **2010,** *132* (46), 16714-16724.
6. Zhang, Z.; Chen, P.; Murakami, T. N.; Zakeeruddin, S. M.; Graetzel, M., The 2,2,6,6-tetramethyl-1-piperidinyloxy radical: An efficient, iodine-free redox mediator for dye-sensitized solar cells. *Advanced Functional Materials* **2008,** *18* (2), 341-346.
7. Daeneke, T.; Kwon, T.-H.; Holmes, A. B.; Duffy, N. W.; Bach, U.; Spiccia, L., High-efficiency dye-sensitized solar cells with ferrocene-based electrolytes. *Nature Chemistry* **2011,** *3* (3), 211-215.
8. Yum, J.-H.; Baranoff, E.; Kessler, F.; Moehl, T.; Ahmad, S.; Bessho, T.; Marchioro, A.; Ghadiri, E.; Moser, J.-E.; Yi, C., A cobalt complex redox shuttle for dye-sensitized solar cells with high open-circuit potentials. *Nature Communications* **2012,** *3*, 631.
9. Chen, C.-Y.; Wang, M.; Li, J.-Y.; Pootrakulchote, N.; Alibabaei, L.; Ngoc-le, C.-h.; Decoppet, J.-D.; Tsai, J.-H.; Grätzel, C.; Wu, C.-G., Highly efficient light-harvesting ruthenium sensitizer for thin-film dye-sensitized solar cells. *Acs Nano* **2009,** *3* (10), 3103-3109.
10. Yella, A.; Lee, H.-W.; Tsao, H. N.; Yi, C.; Chandiran, A. K.; Nazeeruddin, M. K.; Diau, E. W.-G.; Yeh, C.-Y.; Zakeeruddin, S. M.; Grätzel, M., Porphyrin-sensitized solar cells with cobalt (II/III)–based redox electrolyte exceed 12 percent efficiency. *Science* **2011,** *334* (6056), 629-634.
11. Hattori, S.; Wada, Y.; Yanagida, S.; Fukuzumi, S., Blue copper model complexes with distorted tetragonal geometry acting as effective electron-transfer mediators in dye-sensitized solar cells. *Journal of the American Chemical Society* **2005,** *127* (26), 9648-9654.
12. Li, T. C.; Spokoyny, A. M.; She, C.; Farha, O. K.; Mirkin, C. A.; Marks, T. J.; Hupp, J. T., Ni (III)/(IV) bis (dicarbollide) as a fast, noncorrosive redox shuttle for dye-sensitized solar cells. *Journal of the American Chemical Society* **2010,** *132* (13), 4580-4582.
13. Wang, M.; Chamberland, N.; Breau, L.; Moser, J.-E.; Humphry-Baker, R.; Marsan, B.; Zakeeruddin, S. M.; Grätzel, M., An organic redox electrolyte to rival triiodide/iodide in dye-sensitized solar cells. *Nature Chemistry* **2010,** *2* (5), 385-389.
14. Ito, S.; Chen, P.; Comte, P.; Nazeeruddin, M. K.; Liska, P.; Péchy, P.; Grätzel, M., Fabrication of screen-printing pastes from TiO2 powders for dye-sensitised solar cells. *Progress in photovoltaics: research and applications* **2007,** *15* (7), 603-612.

15. http://www.rsc.org/suppdata/nr/c2/c2nr31127e/c2nr31127e.pdf